*Progress In Electromagnetics Research M, Vol. 98, 193–203, 2020*

# Interior Permanent Magnet Synchronous Motor Dead-Time Compensation Combined with Extended Kalman and Neural Network Bandpass Filter

**Lidong Zhu, Ben Xu*, and Huangqiu Zhu**

**Abstract**—In order to overcome the problem of high voltage loss rate caused by the increase of current harmonics due to dead-time effect and the decrease of average potential output of inverter in the control process of the interior permanent magnet synchronous motor (IPMSM) for electric vehicles, a dead-time compensation control method based on an extended Kalman filter (EKF) and a neural network bandpass filter (NNBPF) is proposed. Firstly, from the mechanism of dead-time effect, the problems and causes of dead-time effect are analyzed. Secondly, the extended Kalman filter combining feedback and prediction function is used to filter the $d$- and $q$-axis currents of the motor, so as to solve the problem that zero current polarity is difficult to judge in the traditional dead-time compensation process. Thirdly, the high-order harmonics due to dead-time effect in the $d$- and $q$-axis currents are extracted by using the neural network band-pass filter, and the dead-zone compensation is carried out after the amplitude phase adjustment. Finally, the effectiveness of the proposed dead zone compensation method is proved by comparing no dead-time compensation with the dead-time compensation strategy proposed in this paper. The experimental results show that the proposed dead-time compensation method can effectively suppress the current harmonics, reduce the current distortion, reduce the voltage loss rate to 0.04%, improve the voltage utilization ratio, and effectively improve the operating performance and endurance of electric vehicles.

## 1. INTRODUCTION

Interior permanent magnet synchronous motor (IPMSM) has the advantages of simple structure, small volume, light weight, small loss, and high efficiency, so it is widely used in special vehicles such as electric vehicles. Space vector pulse width modulation (SVPWM) technology is usually used to control and speed regulation IPMSM electric vehicles [1–3]. Ideally, the on and off time of the switch tube is zero, and the upper and lower bridge arms are completely complementary. However, in practice, the turn-off time of the switch tube is longer than that of the conduction time. In order to prevent the situation that the upper and lower bridge arms are turned on at the same time due to the long turn-off time, and the circuit is damaged, the dead zone time is usually introduced before the switch tube is switched on. However, due to the introduction of dead time, the current harmonic component of the inverter output increases, and the pulse width of the output become narrower, resulting in voltage loss.

In order to solve the adverse effect of dead-time effect on motor operation, in-depth research on this is carried out, and a variety of dead-time compensation algorithms are proposed by scholars. A neural network harmonic current loop is added to realize the decomposition and extraction of current harmonics on the basis of the traditional vector control algorithm, and the extracted current harmonics are trained by the neural network to obtain compensation voltage for dead-time compensation in [4, 5];

*Received 9 October 2020, Accepted 16 November 2020, Scheduled 20 November 2020*
* Corresponding author: Ben Xu (benedictor_xu@163.com).
The authors are with the School of Electrical and Information Engineering, Jiangsu University, Zhenjiang 212013, China.

the compensation achieves good results, and the switching frequencies of 5 kHz and 10 kHz in the literature can be realized in low-performance controllers, which have certain values for engineering applications. A comprehensive pulse width modulation method is proposed in [6] where the actual voltage space and fundamental voltage amplitude are effectively expanded, and the method has certain values in practical engineering applications. A low-frequency oscillation suppression strategy based on the combination of current closed-loop and dead-time compensation is proposed in [7]. The low-frequency oscillation of the speed control system is better suppressed, and the stability and speed control performance of the system are both improved. The realization of lower switching frequency has certain values in practical engineering applications. An RRC strategy is proposed in [8] to reduce current harmonics and distortion rate. The current is applied to dead-time compensation, and good compensation effects are achieved. This method has the advantages of simple implementation and good compensation effects. It has certain values in practical engineering applications. A new type of auto-disturbance dead-time compensation method is proposed in [9] and effectively reduces the harmonic content, but this method has the problem of difficulty in tuning parameters, and it is difficult to obtain better applications in actual projects. The voltage error caused by the dead zone effect is analysed in detail, and an online compensation algorithm for the dead time based on the $q$-axis current error is proposed in [10]. An accurate model of the motor and inverter is not required by the algorithm, and the reference current is used to determine the current polarity. However in actual operation, false compensation may be caused by complicated working conditions of the motor. The parasitic capacitance of the power device is considered in the dead-time effect in [11] where the ripple current is calculated to achieve voltage compensation, but the calculation of this algorithm takes a long time and is difficult to apply in practice. The use of Kalman filter algorithm is proposed in [12] to estimate the disturbance voltage to suppress the voltage distortion and torque ripple caused by the 5th and 7th currents of the $\alpha$, $\beta$ coordinate systems and the 6th harmonic currents in the $d$, $q$ coordinate systems, and solves the problem of reduced algorithm efficiency and achieves good results. However, this algorithm has a problem that it is difficult to practically apply to the 62.5 µs control period in the literature.

The dead-time compensation methods mentioned in the above literature have certain application research value, but the judgment of the zero current polarity and the reduction of the voltage loss rate are rarely mentioned. Based on the analysis of the dead-time effect mechanism, this paper proposes a dead-time compensation algorithm combining extended Kalman filter (EKF) and neural network band pass filter (NNBPF). Firstly, the extended Kalman filter (EKF) real-time recursion is used to filter the $d$- and $q$-axis currents in real time, which solves the problem that the polarity of the zero point current under the traditional dead-time compensation algorithm is difficult to distinguish. Secondly, the neural network band-pass filter (NNBPF) is used to extract the harmonic components in the filtered $d$- and $q$-axis currents, and performs harmonic compensation after adjustment. Combined with the traditional dead-time compensation algorithm, the current harmonics are suppressed, and the voltage loss rate is reduced. Finally, the correctness and effectiveness of the proposed method are verified on the experimental platform.

## 2. DEAD-TIME EFFECT AND COMPENSATION METHOD

### 2.1. Dead-Time Effect

As shown in Fig. 1, in order to simplify the analysis, an A-phase bridge arm of the power inverter circuit is taken as an example. In the SVPWM algorithm, complementary SVPWM waves are injected into the upper and lower bridge arms. Ideally, the turn-on and turn-off time of the IGBT of the upper and lower bridge arms is zero, so the upper and lower bridge arms will not be turned on at the same time. However, due to the device characteristics under actual conditions, the turn-off time of the IGBT is slightly longer than the turn-on time. If the on-off is controlled according to an ideal trigger time, the two switch tubes of the same bridge arm may be turned on, and a short circuit occurs. In order to avoid this phenomenon, a delay time must be inserted before the two tubes are turned on. This time is called the dead time. During the dead time, both switching tubes are in the off state. At this time, the load current flows through the freewheeling diode, and the load voltage will not be controlled by the switching tube. At this time, the average voltage output by the inverter decreases, and 3, 5, 7 times and other harmonic components proportional to the dead time and modulation ratio are produced.

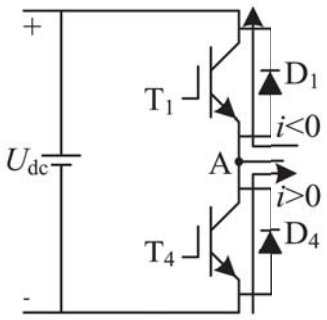


**Figure 1.** Single-phase bridge arm of inverter.

This phenomenon is especially serious when the switching frequency is high, and the load inductance is weak. Assuming that the phase A current $i$ from point A in the figure to the load is positive, during the dead time, when $i > 0$, because the upper and lower switch tubes are in the off state, the inductive load can only complete the freewheeling through the freewheeling diode $D_4$ of the lower bridge arm. At this time, a phase A backpressure $-U_{dc}/2$ is generated. Set the dead time as $T_d$, which means that in a PWM cycle, there is an extra negative potential with a width of $T_d$. At this time, the output voltage value is lower than the expected value, and the positive pulse width is narrowed. When $i < 0$, because the two switch tubes are turned off, the inductive load can only complete the freewheeling through the freewheeling diode $D_1$ of the upper bridge arm. At this time, in each PWM cycle, there is an extra positive potential $U_{dc}/2$ with a width of $T_d$. The output voltage value is higher than the expected value, and the negative pulse width becomes narrower.

In PWM control mode, a reverse pulse due to the dead-time effect will be inserted in each PWM cycle. The pulse width is the dead time $T_d$, and the pulse amplitude is half of the bus voltage amplitude, i.e., $U_{dc}/2$. The equivalent result of the dead zone effect is shown in Fig. 2. Low-order harmonics such as 3, 5, and 7 will be introduced by the reverse pulse, and they cannot be effectively attenuated. Severe waveform distortion is caused to the output voltage. At the same time, the output voltage of the inverter is attenuated, and the voltage loss rate increases.

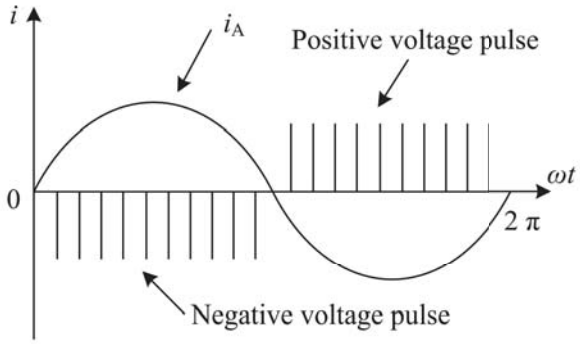


**Figure 2.** Dead time voltage error equivalent principle.

### 2.2. Traditional Dead-time Effect Compensation Method

According to the analysis in the previous section, when the polarity of the phase current is determined, the polarity, phase, and amplitude of the pulse generated by the dead-time effect can be distinguished, and thus the low order harmonics such as 3, 5, 7 and the potential lost by the inverter output voltage are uniquely determined. For a certain current direction, there is only one switch tube in the same group

of bridge arms to control the output voltage. Even if the other switch tube is turned on, it will only flow through its freewheeling diode. Therefore, if the direction of the phase current can be accurately determined, by increasing or decreasing the turn-on time of the switch tube that controls the output voltage, the potential loss caused by the dead time can be compensated.

The traditional dead zone compensation method also takes the A-phase bridge arm in Fig. 1 as an example. When the phase current $i > 0$, the upper bridge arm conduction time is extended, and the complementary lower bridge arm conduction time is shortened accordingly; when the phase current $i < 0$, the conduction time of the lower bridge arm is extended, and the conduction time of the complementary upper bridge arm is shortened accordingly. When PWM is in the edge alignment mode, the value of each compensation is equal to the width of the dead time. When the PWM is in the center alignment mode, the value of each compensation is half the width of the dead time.

The key of dead time compensation is to accurately determine the polarity of the current. The traditional dead time compensation method phase current polarity detection is usually realized by the hardware circuit as shown in Fig. 3. The working principle of the circuit is: Firstly, the AC voltage signal is obtained by $i_A$ via $R_1$, and high-order harmonics are filtered out through a low-pass filter. Then the signal is passed through a high-pass filter to filter out the DC component on the one hand and compensate for the phase lag caused by the low-pass filter on the other hand. Finally, the obtained signal is compared with the zero point to output a square wave signal with a duty cycle of 50%, which is isolated and input to the controller via a linear high-speed optocoupler to realize the judgment of the phase current polarity. However, the hardware filtering has poor steepness, i.e., poor signal selectivity. In the vicinity of zero current, the polarity of the current is prone to misjudgment, which leads to miscompensation.

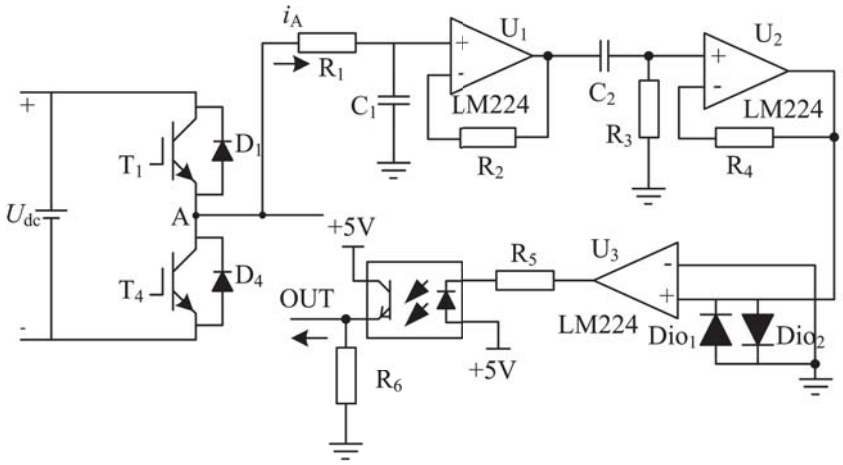


**Figure 3.** Phase current polarity detection circuit.

## 3. DESIGN OF CONTROLLER

### 3.1. Design of EKF Current Filter

The traditional dead time compensation algorithm based on current polarity judgment has the characteristics of easy realization, high efficiency, and good compensation effect, so it is widely used in practical engineering. However, when the phase current is near zero, due to the characteristic of poor selectivity of hardware filtering, the accuracy of judging current polarity is low, and error compensation occurs easily, which leads to the increase of current harmonics near zero current and the aberration of current waveform. To solve this problem, an extended Kalman filter (EKF) is used to filter the sampled axis current in real time, so as to improve the accuracy of current polarity discrimination. Combined with traditional dead time compensation algorithm mentioned in [7], the filtered current is calculated, and the voltage is compensated.

Assuming that the inductance and resistance of IPMSM are constants and ignoring their changes with temperature, using stator current and stator voltage as state variables, construct the IPMSM mathematical model in the $d$-$q$ coordinate system:

$$\begin{cases} pi_d = -\dfrac{R_\mathrm{s}}{L_d} i_d + \omega_\mathrm{e} \dfrac{L_q}{L_d} i_q + \dfrac{u_d}{L_d} \\ pi_q = -\dfrac{R_\mathrm{s}}{L_q} i_q - \omega_\mathrm{e} \dfrac{L_d}{L_q} i_d + \dfrac{u_q}{L_q} - \omega_\mathrm{e} \dfrac{\psi_\mathrm{f}}{L_q} \end{cases} \tag{1}$$

where $p$ represents the differential operator; $L_d$ and $L_q$ represent $d$ and $q$ axis inductors; $u_d$ and $u_q$ represent $d$ axis and $q$ axis voltages; $i_d$ and $i_q$ represent $d$- and $q$-axis currents; $R_\mathrm{s}$ represents the stator resistance; $\psi_\mathrm{f}$ represents the permanent magnet flux; $\omega_\mathrm{e}$ represents the electric angular velocity of the motor.

Formula (1) is rewritten as a discrete state space equation [13, 14]:

$$\begin{cases} \boldsymbol{x}(k+1) = \boldsymbol{A'}\boldsymbol{x}(k) + \boldsymbol{B'}\boldsymbol{u}(k) \\ \boldsymbol{y}(k) = \boldsymbol{C'}\boldsymbol{x}(k) \end{cases} \tag{2}$$

where T represents the controller sampling time, and the coefficients are:

$$\boldsymbol{A'} = \begin{bmatrix} 1 - T\dfrac{R_\mathrm{s}}{L_d} & \omega_\mathrm{e} T \dfrac{L_q}{L_d} \\ -\omega_\mathrm{e} T \dfrac{L_d}{L_q} & 1 - T\dfrac{R_\mathrm{s}}{L_q} \end{bmatrix}, \quad \boldsymbol{B'} = \begin{bmatrix} \dfrac{T}{L_d} & 0 \\ 0 & \dfrac{T}{L_q} \end{bmatrix}, \quad \boldsymbol{C'} = \begin{bmatrix} 1 & 0 \\ 0 & 1 \end{bmatrix},$$

$$\boldsymbol{x} = [i_d, i_q]^\mathrm{T}, \quad \boldsymbol{u} = [u_d, u_q]^\mathrm{T}, \quad \boldsymbol{y} = [i_d, i_q]^\mathrm{T}$$

Order $f[\boldsymbol{x}(k)] = \boldsymbol{A'}\boldsymbol{x}(k)$, $g[\boldsymbol{x}(k)] = \boldsymbol{C'}\boldsymbol{x}(k)$. Then the relevant matrices are:

$$\boldsymbol{F}(k+1) = \frac{\partial f(\boldsymbol{x})}{\partial \boldsymbol{x}} = \begin{bmatrix} 1 - T\dfrac{R_\mathrm{s}}{L_d} & \omega_\mathrm{e}(k) T \dfrac{L_q}{L_d} \\ -\omega_\mathrm{e}(k) T \dfrac{L_d}{L_q} & 1 - T\dfrac{R_\mathrm{s}}{L_q} \end{bmatrix} \tag{3}$$

$$\boldsymbol{G}(k+1) = \frac{\partial g(\boldsymbol{x})}{\partial \boldsymbol{x}} = \begin{bmatrix} 1 & 0 \\ 0 & 1 \end{bmatrix} \tag{4}$$

Combined with the above formula, the extended Kalman current filtering algorithm can be divided into three stages, namely the prediction stage, gain matrix calculation stage, and correction update stage.

In the prediction stage, according to the equation of state and the current obtained after filtering, the predicted currents of the $d$- and $q$-axes and a priori estimated covariance are calculated:

$$\begin{cases} \tilde{\boldsymbol{x}}(k+1) = \boldsymbol{A'}\hat{\boldsymbol{x}}(k) + \boldsymbol{B'}\boldsymbol{u}(k) \\ \tilde{\boldsymbol{P}}(k+1) = \boldsymbol{F}(k+1)\hat{\boldsymbol{P}}(k)\boldsymbol{F}^\mathrm{T}(k+1) + \boldsymbol{Q} \end{cases} \tag{5}$$

where $\tilde{\boldsymbol{x}}$ represents $d$, $q$ axis current forecast; $\hat{\boldsymbol{x}}$ represents the current value of filtered $d$, $q$ axes; $\tilde{\boldsymbol{P}}(k+1)$ represents the priori estimated covariance at $k+1$; $\hat{\boldsymbol{P}}(k)$ represents the posterior estimated covariance at $k$; $\boldsymbol{Q}$ represents the system noise covariance matrix.

In the gain matrix calculation stage, the Kalman gain matrix is calculated using the estimated covariance calculated in the prediction stage:

$$\boldsymbol{K}(k+1) = \tilde{\boldsymbol{P}}(k+1)\boldsymbol{G}^\mathrm{T}(k+1)\left[\boldsymbol{G}(k+1)\tilde{\boldsymbol{P}}(k+1)\boldsymbol{G}^\mathrm{T}(k+1) + \boldsymbol{R}\right]^{-1} \tag{6}$$

where $\boldsymbol{R}$ represents the covariance matrix of measurement noise.

The correction update stage is mainly responsible for outputting the $d$, $q$ axis prediction currents of the period, and updating the filtered $d$, $q$ axis current values and the prior estimation covariance of the next period:

$$\begin{cases} \tilde{\boldsymbol{y}}(k+1) = \boldsymbol{C'}\tilde{\boldsymbol{x}}(k+1) \\ \hat{\boldsymbol{x}}(k+1) = \tilde{\boldsymbol{x}}(k+1) + \boldsymbol{K}(k+1)(\boldsymbol{y}(k+1) - \tilde{\boldsymbol{y}}(k+1)) \\ \hat{\boldsymbol{P}}(k+1) = (\boldsymbol{I} - \boldsymbol{K}(k+1)\boldsymbol{G}(k+1))\tilde{\boldsymbol{P}}(k+1) \end{cases} \tag{7}$$

After the update is completed, the filtered $d$, $q$ axis current values $\hat{\boldsymbol{x}}(k+1)$ at $k+1$ are output, and priori estimated covariance $\hat{\boldsymbol{P}}(k+1)$ will participate in the prediction of the next cycle. Iterate continuously and filter in real time to improve the accuracy of the detection current, thereby improving the accuracy of judging current polarity near zero current.

### 3.2. Design of NNBPF

According to the $d$-$q$ coordinate system, the harmonic order of the current generated by the dead-time effect is mainly 6 and 12 times. Firstly, write the current expressions of $d$- and $q$-axes:

$$\begin{cases} \Delta i_d = \omega_{d6_1}\cos(6\theta_{\mathrm{e}}) + \omega_{d6_2}\sin(6\theta_{\mathrm{e}}) + \omega_{d12_1}\cos(12\theta_{\mathrm{e}}) + \omega_{d12_2}\sin(12\theta_{\mathrm{e}}) \\ \Delta i_q = \omega_{q6_1}\cos(6\theta_{\mathrm{e}}) + \omega_{q6_2}\sin(6\theta_{\mathrm{e}}) + \omega_{q12_1}\cos(12\theta_{\mathrm{e}}) + \omega_{q12_2}\sin(12\theta_{\mathrm{e}}) \end{cases} \tag{8}$$

where $\omega_{d6_1}$, $\omega_{q6_1}$ and $\omega_{d6_2}$, $\omega_{q6_2}$ represent the amplitude of cosine component and amplitude of sine component of the 6th harmonic of $d$, $q$ axis currents, respectively; $\omega_{d12_1}$, $\omega_{q12_1}$ and $\omega_{d12_2}$, $\omega_{q12_2}$ represent the amplitude of cosine component and amplitude of sine component of the 12th harmonic of $d$, $q$ axis currents, respectively. The amplitude of these components is also the weight of the neural network bandpass filter. Weights are adjusted online using a least mean square (LMS) algorithm with small computation and fast convergence.

Define the cost function:

$$\begin{aligned} J &= \left(\hat{i}_d - i_{d\mathrm{h}}\right)^2 + \left(\hat{i}_q - i_{q\mathrm{h}}\right)^2 \\ &= e_d^2 + e_q^2 \end{aligned} \tag{9}$$

where $\hat{i}_d$, $\hat{i}_q$ represent the output $d$, $q$ axis currents of EKF, and $e_d$, $e_q$ represent $d$, $q$ axis error currents.

In order to make the weights converge to an accurate value, the weights can be updated along the negative direction of the partial derivative of the cost function with respect to each weight, and then the cost function is reduced to achieve the purpose of convergence. The partial derivative of the cost function with respect to each weight is:

$$\begin{cases} \dfrac{\partial J}{\partial \boldsymbol{\omega}_d} = -2e_d \cdot \boldsymbol{r} \\ \dfrac{\partial J}{\partial \boldsymbol{\omega}_q} = -2e_q \cdot \boldsymbol{r} \end{cases} \tag{10}$$

After that, the weight value of the harmonic current of the $d$, $q$ axes is updated according to the weight updating rule. The weight updating rule is as follows:

$$\begin{cases} \boldsymbol{\omega}_d(k+1) = \boldsymbol{\omega}_d(k) + 2\mu e_d(k)\,\boldsymbol{r}(k) \\ \boldsymbol{\omega}_q(k+1) = \boldsymbol{\omega}_q(k) + 2\mu e_q(k)\,\boldsymbol{r}(k) \end{cases} \tag{11}$$

where $\boldsymbol{\omega}_d = [\omega_{d6_1}, \omega_{d6_2}, \omega_{d12_1}, \omega_{d12_2}]^T$, $\boldsymbol{\omega}_q = [\omega_{q6_1}, \omega_{q6_2}, \omega_{q12_1}, \omega_{q12_2}]^T$, $\boldsymbol{r} = [\cos 6\theta_e, \sin 6\theta_e, \cos 12\theta_e, \sin 12\theta_e]^T$, $\mu$ represents the learning rate.

The 6th and 12th harmonic components in axis current can be obtained according to the designed neural network bandpass filter. The obtained harmonic current is converted into dead-time compensation voltage by PI regulator $u_{dhcom}$ and $u_{qhcom}$, and the dead time compensation method of current polarity discrimination is compensated twice by this method. The $d$-axis NNBPF dead time compensation algorithm is given here, and its structure is shown in Fig. 4.

64 multiplications, 45 additions, and 4 division instructions are used in the EKF current filtering algorithm. 32 multiplications, 16 additions, and 8 trigonometric function instructions are used in the NNBPF dead time compensation algorithm. Taking the MCU used in this article as an example, its main frequency is 100 MHz, and the time to execute an EKF algorithm and NNBPF algorithm is about 8 µs and 6 µs, so the real-time performance can meet the control requirements. According to the analysis and design above, the dead time compensation algorithm block diagram of the electric drive system as shown in Fig. 5 can be drawn.

In the algorithm block diagram shown in Fig. 5, the axis current $i_d$ and $i_q$ are filtered by EKF firstly, and the axis current was directly fed back to the forward path and the NNBPF dead time compensation

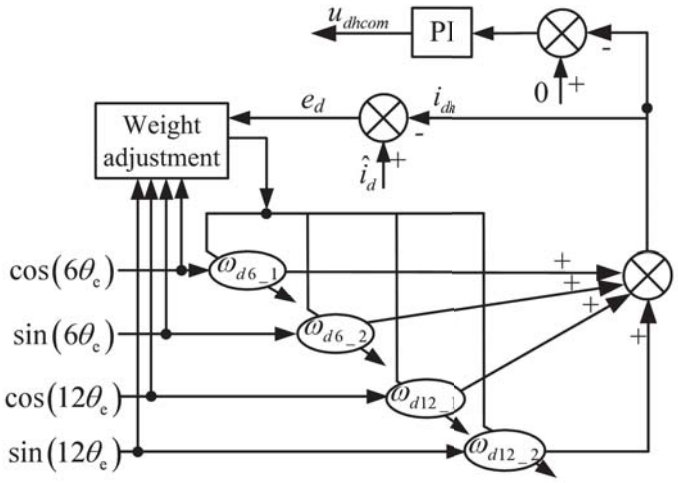


**Figure 4.** Structure diagram of $d$-axis NNBPF dead time compensation algorithm.

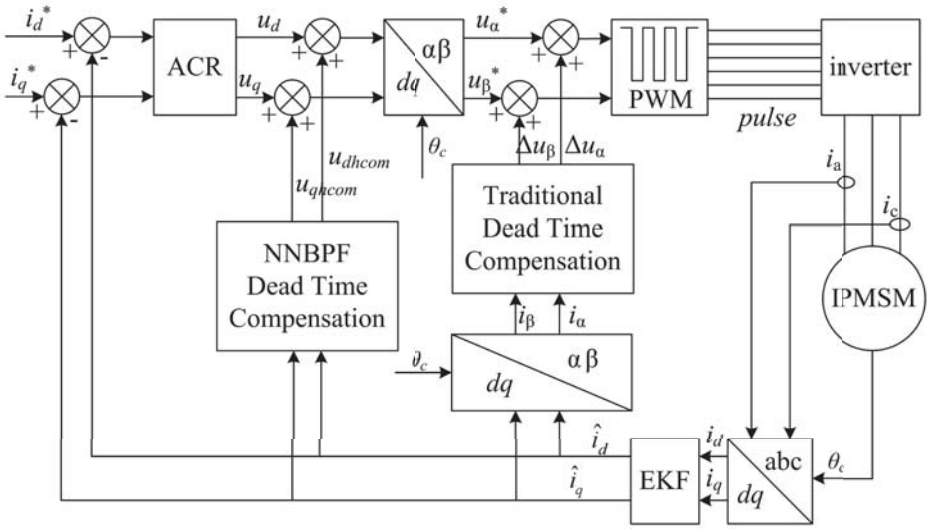


**Figure 5.** Block diagram of dead time compensation control for electric drive system.

algorithm, and the filtered current was converted to $\hat{i}_d$ and $\hat{i}_q$, then $\hat{i}_d$ and $\hat{i}_q$ were used for the traditional dead time compensation algorithm, then the $u_{dhcom}$ and $u_{qhcom}$ calculated by the NNBPF dead time compensation algorithm and $\Delta u_\alpha$, $\Delta u_\beta$ calculated by the traditional dead time compensation algorithm were used for dead time voltage compensation.

## 4. EXPERIMENTAL VERIFICATION

In order to verify the correctness of the proposed method, the experimental platform shown in Fig. 6 is constructed, and the waveforms of the dead time compensation algorithm and the no dead time compensation algorithm in this paper are compared and analyzed. In Fig. 6, the electric dynamometer and the prototype are coupled and operated in the electric state. At this time, the motor is in the torque control mode, and the given torque is $10\,\mathrm{N}\cdot\mathrm{M}$. Since the dead time effect is particularly obvious at low speeds, the speed of the electric dynamometer is set to 10% of the rated speed of the prototype, which is $360\,\mathrm{r/min}$. The parameters of the current loop PI controller in the controller are respectively: $k_p$ of $d$-axis is 0.7, and $k_i$ of $d$-axis is 0.01; $k_p$ of $q$-axis is 1.5, and $k_i$ of $q$-axis is 0.02. The PI controller

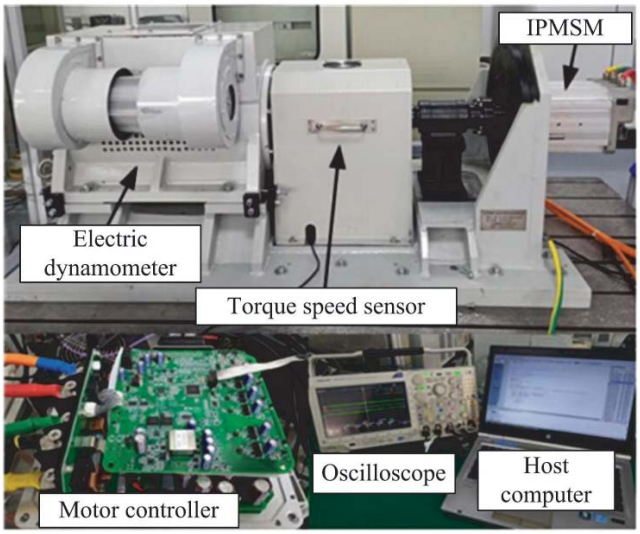


**Figure 6.** Platform of IPMSM control system.

parameters in the NNBPF dead effect compensation algorithm are: $k_p$ is 1; $k_i$ is 0.5; and $\mu$ is 0.001. In order to suppress the influence of harmonics in the current, the system noise covariance matrix of EKF is $\boldsymbol{Q} = \text{diag}[0.01, 0.01]$, and the measurement noise covariance matrix is $\boldsymbol{R} = \text{diag}[50, 50]$.

The main parameters of IPMSM and inverter are shown in Table 1.

**Table 1.** IPMSM and power device parameters.

| | Parameters | Value |
|---|---|---|
| Motor | Stator resistance $R_\text{s}$ ($\Omega$) | 0.006 |
| | Stator inductance $L_d$ (H) | 0.00005 |
| | Stator inductance $L_q$ (H) | 0.00012 |
| | Pole Pairs | 4 |
| | Permanent magnet flux $\psi_\text{f}$ (Wb) | 0.03951 |
| | Rated power $P$ (kW) | 20 |
| | Rated voltage $U$ (V) | 67 |
| | Rated current $I$ (A) | 180 |
| | Rated torque $T_\text{e}$ ($\text{N} \cdot \text{m}$) | 54 |
| Power component | Turn-off delay time $T_\text{f}$ (ns) | 80 (25°) |
| | Opening delay time $T_r$ (ns) | 91 (25°) |
| | Switching frequency $T_\text{PWM}$ (kHz) | 10 |
| | Dead time $T_d$ ($\mu$s) | 5 |

The phase current spectrogram in the motor windings corresponding to the no dead time effect compensation algorithm, the traditional dead time effect compensation algorithm, and the proposed NNBPF-EKF dead time effect compensation are shown in Fig. 7. The output voltage of the controller (theoretical output voltage of the inverter), phase voltage of the motor (actual output voltage of the inverter), voltage loss (the difference between the output voltage of the controller and the phase voltage of the motor), and the voltage loss rate (the percentage of the voltage loss to the DC bus voltage) are

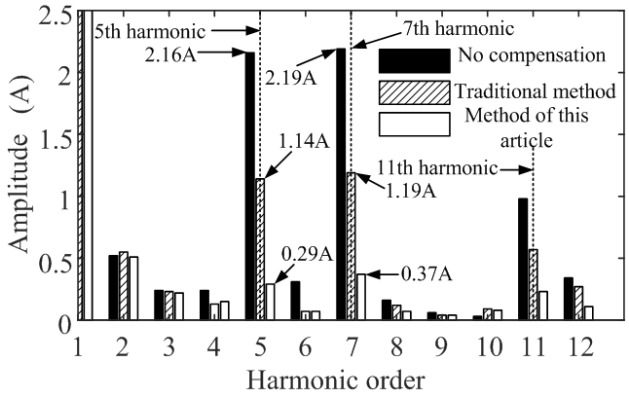


**Figure 7.** Phase current spectrum.

shown in Table 2. The DC bus voltage used in the experiment is 96 V. In Fig. 7, the situation without dead time effect compensation is represented by the solid histogram. The 5th, 7th, and 11th phase current harmonic amplitudes without dead time effect compensation are 2.16 A, 2.19 A, and 0.98 A, respectively. At this time, the voltage loss is 6.33 V in Table 2, and the voltage loss rate is 6.59%. The traditional dead zone compensation algorithm is represented by the shaded histogram. The 5th, 7th, and 11th phase current harmonic amplitudes of the traditional dead zone compensation method are 1.14 A, 1.19 A, and 0.57 A, respectively, and the amplitudes are reduced to none. 52.78%, 54.34%, and 58.16% of the compensation method. At this time, the voltage loss is 0.88 V in Table 2, and the voltage loss rate is 0.92%. The method proposed in this paper is represented by the hollow histogram. The 5th, 7th, and 11th phase current harmonic amplitudes of the proposed dead time compensation method are 0.29 A, 0.37 A, and 0.23 A, respectively. The amplitude is reduced to 13.43%, 16.89%, and 23.47% of the uncompensated method, respectively. At this time, the voltage loss is 0.04 V in Table 2, and the voltage loss rate is 0.04%.

**Table 2.** Voltage loss rate.

| | Controller output voltage (V) | Motor phase voltage (V) | Voltage loss (V) | Voltage loss rate |
|---|---|---|---|---|
| No compensation | 9.83 | 3.50 | 6.33 | 6.59% |
| Traditional Method | 4.38 | 3.50 | 0.88 | 0.92% |
| Method of this article | 3.54 | 3.50 | 0.04 | 0.04% |

The spectrum of $d$-axis current corresponding to the no dead time effect compensation algorithm, traditional dead time effect compensation algorithm, and the proposed NNBPF-EKF dead time effect compensation are shown in Fig. 8. In Fig. 8, the situation without dead time compensation is represented by the solid histogram. The 6th and 12th harmonic amplitudes of $d$-axis current without dead time compensation are 3.56 A and 1.60 A, respectively. The traditional dead zone compensation method is represented by the shaded histogram. The 6th and 12th $d$-axis current harmonic amplitudes of the traditional dead zone compensation method are 1.45 A and 0.91 A, respectively, and the amplitudes are reduced to 40.73% and 56.88% of the uncompensated method. The method proposed in this paper is represented by the hollow histogram. The 6th and 12th harmonic amplitudes of $d$-axis current in the proposed dead time compensation method are 0.75 A and 0.36 A, respectively. The amplitude is reduced

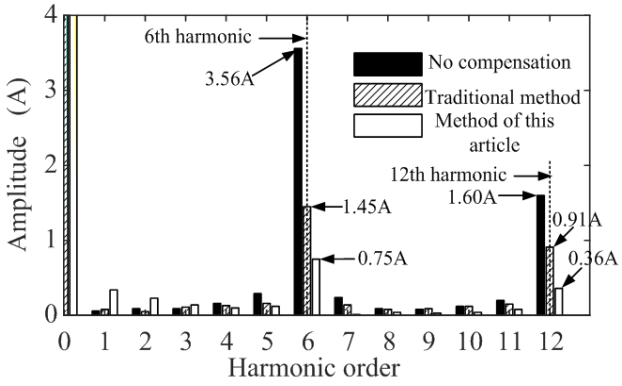


**Figure 8.** $d$-axis current spectrum.

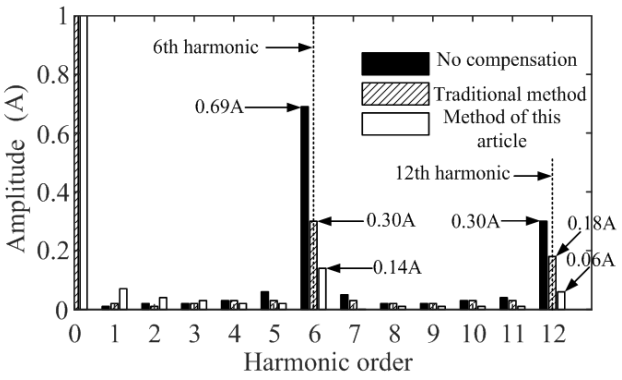


**Figure 9.** $q$-axis current spectrum.

to 21.07% and 22.50% of the uncompensated method, respectively.

The spectrum of $q$-axis current corresponding to the no dead time effect compensation algorithm, the traditional dead time effect compensation algorithm, and the proposed NNBPF-EKF dead time effect compensation are shown in Fig. 9. In Fig. 9, the situation without dead time compensation is represented by the solid histogram. The amplitudes of the 6th and 12th $q$-axis current harmonics without dead time compensation are 0.69 A and 0.30 A, respectively. The traditional dead zone compensation method is represented by the shaded histogram. The amplitudes of the 6th and 12th $q$-axis current harmonics of the traditional dead zone compensation method are 0.30 A and 0.18 A, respectively, and the amplitudes are reduced to 43.48% and 60.00% of those without compensation. The method proposed in this paper is represented by the hollow histogram. The 6th and 12th harmonic amplitudes of $q$-axis current in the proposed dead time compensation method are 0.14 A and 0.06 A, respectively. The amplitude is reduced to 20.29% and 20.00% of the uncompensated method, respectively.

Compared with the no dead time compensation method and the traditional dead time compensation method, the proposed dead time voltage compensation method combined with extended Kalman filter and neural network band-pass filter has better suppression in the current harmonic amplitude, harmonic component, and voltage loss rate, which makes the electric drive system have better control performance.

## 5. CONCLUSIONS

Aiming at the problems of high current harmonics and high voltage loss rate caused by dead time effect of IPMSM for electric vehicles, a dead time compensation method combining extended Kalman filter and neural network band-pass filter is proposed in this paper. Firstly, the $d$- and $q$-axis currents are filtered by using the characteristics of real-time recursive filtering of extended Kalman filter. The current polarity discrimination near zero currents of $d$- and $q$-axes is improved. Secondly, the harmonic components of $d$- and $q$-axis currents after Kalman filtering are extracted through a neural network band-pass filter. The weight of harmonic is determined by the least mean square algorithm, and then the harmonic compensation is carried out after adjustment. Finally, by comparing the dead time compensation method in this article with the no dead time compensation method and traditional dead time compensation method, it is proved that the dead time compensation method proposed in this paper can make the $d$- and $q$-axis currents have smaller harmonics and reduce the voltage loss rate to 0.04%, which effectively improves the operation performance and driving range of electric vehicles.

## ACKNOWLEDGMENT

This work was supported in part by the National Natural Science Foundation of China (61973144), in part by the Priority Academic Program Development of Jiangsu Higher Education Institutions (PAPD-2018-87).

## REFERENCES


1. Liu, G.-H., G.-H. Xu, W.-X. Zhao, et al., "Improvement of torque capability of permanent-magnet motor by using hybrid rotor configuration," *IEEE Transactions on Energy Conversion*, Vol. 32, No. 3, 2017.
2. Zhou, H.-W., Z. Lu, W.-X. Zhao, et al., "Design and analysis of low-cost tubular fault-tolerant interior permanent-magnet motor," *IEEE Transactions on Magnetics*, Vol. 52, No. 7, 1–4, 2016.
3. Zhu, X.-Y., W.-Y. Wu, S. Yang, et al., "Comparative design and analysis of new type of flux-intensifying interior permanent magnet motors with different $Q$-axis rotor flux barriers," *IEEE Transactions on Energy Conversion*, Vol. 33, No. 4, 2260–2269, 2018.
4. Wang, S. and J.-S. Kang, "Harmonic extraction and suppression method of permanent magnet synchronous motor based on adaptive linear neural network," *Transactions of China Electrotechnical Society*, Vol. 34, No. 04, 654–663, 2019.
5. Qiu, T., X. Wen, and F. Zhao, "Adaptive linear neuron based dead time effects compensation scheme," *IEEE Transactions on Power Electronics*, Vol. 31, No. 3, 2530–2538, 2015.
6. Huang, Z.-B., L.-R. You, Z.-D. Wang, and X.-Q. Wen, "A novel integrated PWM strategy considering dead-time and minimum pulse-width limitation," *Transactions of China Electrotechnical Society*, Vol. 29, No. 12, 11–18, 2014.
7. Qiao, M.-Z., Y.-H. Xia, and P. Zhu, "Low-frequency oscillation restrain method of induction motor fed by inverter based on current close-loop and dead-time compensation," *Transactions of China Electrotechnical Society*, Vol. 29, No. 11, 126–133, 2014.
8. Tang, Z. and A. Bilal, "Suppression of dead-time distortion through revised repetitive controller in PMSM drives," *IEEE Transactions on Energy Conversion*, Vol. 32, No. 3, 918–930, 2017.
9. Rong, Z.-L. and Q.-J. Chen, "Torque ripple suppression method of PMSM based on ADRC with dead-time compensation," *Control and Decision*, Vol. 31, No. 4, 667–672, 2016.
10. Han, K., X. Sun, B. Liu, et al., "Dead-time on-line compensation scheme of SVPWM for permanent magnet synchronous motor drive system with vector control," *Proceeding of the CSEE*, Vol. 38, No. 2, 620–627, 2018.
11. Li, H.-M., S.-H. Hou, and H.-Y. Yao, "The inverter dead-time compensation of surface mounted permanent magnet synchronous motor drive system based on ripple current calculation," *Transactions of China Electrotechnical Society*, Vol. 32, No. S2, 34–41, 2017.
12. Ludek, B. and O. Lukas, "Compensation of dead-time effects based on kalman filter for PMSM drives," I*FAC-Papers On Line*, Vol. 51, No. 6, 18–23, 2018.
13. Zhang, D. and J.-G. Jiang, "Sensorless control of PMSM for DC micro-grid flywheel energy storage based on EKF," *The Journal of Engineering*, Vol. 2019, No. 16, 1227–1231, 2019.
14. Quang, N. K., N. T. Hieu, and Q. P. Ha, "FPGA-based sensorless PMSM speed control using reduced-order extended Kalman filters," *IEEE Transactions on Industrial Electronics*, Vol. 61, No. 12, 6574–6582, 2014.